Research and Simulation of Regenerative Braking System Using PMSM Motor with FOC Control Method Applying SVPWM Algorithm

Vu Hai Quan[1], Nguyen Trong Duc[2,*], and Hoang Quang Tuan[1]

[1] School of Mechanical Automotive Engineering, Hanoi University of Industry, Vietnam
[2] Moscow Automobile and Road Construction State Technical University (MADI), Moscow 125319, Russia Federation
Email: quanvh@haui.edu.vn (V.H.Q.); nguyentrongduc221999@gmail.com (N.T.D.); tuanhq@haui.edu.vn (H.Q.T.)
*Corresponding author

***Abstract*—Electric Vehicles (EVs) offer a promising solution to reduce reliance on fossil fuels and mitigate environmental pollution. However, maximizing driving range remains a key challenge. Regenerative braking, a technology that recovers kinetic energy typically lost as heat during deceleration, can significantly improve EV efficiency. This research investigates the design and performance of a regenerative braking system for the VinFast VF8 2023 Standard Edition, employing a Permanent Magnet Synchronous Motor (PMSM) controlled via Field-Oriented Control (FOC) and space vector pulse width modulation (SVPWM). The system modeled in MATLAB, includes lithium-ion battery, inverter and PMSM. The simulation utilizes the Federal Test Procedure-75 (FTP-75) drive cycle, focusing on a 40-second segment representative of urban driving. Results demonstrate that during braking phases (0–20 s and 33–40 s), negative input torque causes the PMSM to function as a generator, charging the battery and increasing its capacity by roughly 0.003%. Conversely, during acceleration (20–33 s), positive torque drives the PMSM as a motor, consuming battery power and decreasing capacity by approximately 0.01%. While seemingly modest over the short test period, these findings highlight the potential of regenerative braking to recapture energy and contribute to extending the driving range of the VinFast VF8, demonstrating the feasibility and potential of this energy recovery approach.**

***Keywords*—electric vehicle, regenerative braking system, permanent magnet synchronous motor, field-oriented control lithium-ion battery, state of charge, VinFast VF8**

I. Introduction

According to the World Health Organization's 2023 report on global road safety and as further detailed in Wang *et al.* [1]. In 2021, an estimated 1.19 million deaths were attributed to road traffic crashes globally. This translates to approximately 15 road traffic deaths per 100,000 people. Children and young people (aged 5–29) remain the most vulnerable to road traffic fatalities. In 2019, this age group accounted for the highest proportion of road traffic deaths. Globally, road traffic injuries were the 12th leading cause of death across all age groups. The report, drawing on data from the World Health Organization [2], provides further insights into the global distribution of road traffic fatalities:

a) Occupants of four-wheeled vehicles represent 30% of fatalities.
b) Pedestrians account for 23% of fatalities.
c) Powered two- and three-wheeled vehicle users comprise 21% of fatalities.

The recovery from the COVID-19 pandemic and the global energy crisis has significantly spurred clean energy investment. By 2023, approximately $2.8 trillion was projected to be invested in energy globally. Over $1.7 trillion of this investment was anticipated to be directed towards clean energy technologies, including renewables, nuclear power, grid infrastructure, energy storage, low-emission fuels, energy efficiency improvements and electrification of end-use applications [3, 4].

The recovery from the COVID-19 pandemic and the global energy crisis have significantly boosted investment in clean energy. The article "Overview of Renewable Energy Power Generation and Conversion (2015–2023)" by Eze *et al.* [3] notes that approximately $2.8 trillion was invested in energy in 2023. Of this amount, over $1.7 trillion was projected for clean energy technologies, including renewables, nuclear power, grid infrastructure, energy storage, low-emission fuels, and efficiency improvements, as well as electrification of end-use applications [4].

Electric Vehicles (EVs) [5, 6] have seen significant development and widespread adoption in recent years, including in Vietnam and Russia [7] and globally. Regenerative braking systems enhance EV range by 8–25%. Beyond range extension and energy savings, these systems also contribute to more effective braking control.

During urban driving cycles, cars tend to start and stop more frequently than during highway driving cycles. When braking frequently during an urban driving cycle, more energy is lost. According to the laws of physics, we

Manuscript received October 22, 2024; revised November 28, 2024; accepted December 20, 2024; published April 8, 2025.

cannot recover all of the lost kinetic energy, but we can still convert and store a significant amount of this kinetic energy in batteries or supercapacitors. The recovered energy improves the fuel economy of vehicles and helps extend the range of electric vehicles.

According to a survey on urban and highway driving, it was found that cars tend to start and stop more often in urban areas than when traveling on the highway. More energy is lost when brakes are applied frequently during an urban driving cycle. When applying the principles of motion energy in physics, we realize that it is impossible to recover all the kinetic energy lost during vehicle motion. However, a significant amount of this kinetic energy can be converted and stored in batteries. This leads to improved fuel economy in conventional vehicles and extended operating ranges for electric vehicles.

According to mechanical theory, reverse torque is applied to the wheels when the brake pedal is pressed. Similarly, regenerative braking is based on the principle that vehicle speed is reduced by generating a negative torque (opposing motion) in the motor with the help of the engine controller. In this study, the author focuses on modeling and simulating a regenerative braking system using a permanent magnet synchronous motor. The motor control system design applies the Field-Oriented Control (FOC) method using Space Vector Pulse Width Modulation (SVPWM) algorithms for speed control and energy storage in lithium-ion batteries.

II. Theory of Permanent Magnet Synchronous Motor

Permanent Magnet Synchronous Motors (PMSM) have many advantages over other types of Alternating Current (AC) motors of the same capacity, such as small size, high efficiency and high-power factor. Consequently, they have been widely used in industry and electric cars. To control the PMSM, both sinusoidal PWM (SPWM) and space-vector PWM (SVPWM) can be used to create the necessary 3-phase voltage. SVPWM is more advanced and provides better DC bus voltage utilization [8], thereby reducing harmonic distortion. A PMSM motor [9] consists of an outer stator with conductors and a rotor with permanent magnets. Based on research from two articles by the authors Chengyuan He and Abdelli Abdenour [10, 11], PMSM motors can be classified into two main groups based on their rotor structure:

1. Surface-Mounted PMSM (SPMSM): Permanent magnets are mounted on the rotor surface.

2. Interior PMSM (IPMSM): Permanent magnets are embedded within the rotor.

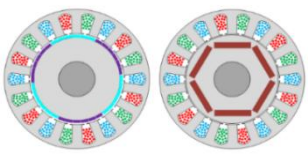

(a) (b)

Fig. 1. Illustrates two basic types of PMSM: (a) SPMSM and (b) IPMSM.

SPMSM is shown in Fig. 1(a). A permanent magnet is mounted on the surface of the rotor shaft and the SPMSM had an evenly distributed air gap. This property makes the axial and transaxial inductances equal (i.e., $L_d = L_q$).

A. The Mathematical Model of PMSM Based on d-q Coordinate System

The most common method for analyzing the electric control of PMSM is the *d-q* axis mathematical model. The mathematical model of the PMSM in the *d-q* reference frame is as follows [12–14]:

The voltage equation:

$$u_d = p\phi_d - \phi_q\omega + R_s i_d \tag{1}$$

$$u_q = p\phi_q + \phi_d\omega + R_s i_q \tag{2}$$

The stator flux linkage equation:

$$\phi_d = L_d i_d + \phi_m \tag{3}$$

$$\phi_q = L_q i_q \tag{4}$$

The electromagnetic torque equation:

$$T_e = \frac{3}{2} p[\phi_m i_q + (L_d - L_q) i_d i_q \tag{5}$$

In this study, the author uses SPMSM when $L_d = L_q$ or when controlled by $i_d = 0$. Then,(5) becomes

$$T_e = \frac{3}{2} p\phi_m i_q \tag{6}$$

Angular velocity is obtained from equation of motion:

$$\frac{d}{d_t}\omega = \frac{1}{J}(T_e - T_f - F\omega_m - T_m) \tag{7}$$

where u_d, u_q: Applied d-q-axis control voltage; i_d, i_q: Stator *d-q*-axis current; ϕ_d, ϕ_q: *d-q*-axis flux linkage; T_m: Mechanical torque on the shaft; ϕ_m: Permanent Magnet (PM) flux linkage; F: Viscous friction; p: Pole-pair numbers of the motor; L_d, L_q: d-q-axis inductance; T_e: Electromagnetic torque; ω: Electrical angular speed; J: Moment of Inertia; T_f: Static friction torque on the shaft.

B. Theory of Permanent Magnet Synchronous Motor Control

Space Vector Pulse-Width Modulation (SVPWM) are the most widely used methods. According to the author's research [15], opinions have been given to confirm that SVPWM is a widely used program in high-precision electric drive systems. Some advantages can be given as follows: 1) Through a complex coordinate transformation process-SVPWM synthesizes the necessary spatial voltage vector; 2) Smooth torque output; 3) Wide speed ranges; 4) High load capacity at low speed and high starting performance.

Sumitra *et al.* [16] have given some advantages of Flux-Oriented Control (FOC) (The FOC structure with space vector pulse width modulation control algorithm is shown in Fig. 2.) as follows: a) FOC converts the transformation

of a complex and coupled AC model into a simple linear system; b) independent control of torque and flux; c) Fast dynamic response, high steady state performance; d) High torque and low current at start-up.

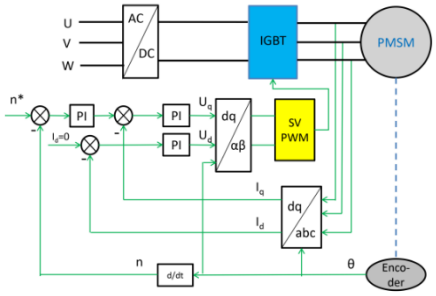

Fig. 2. Structure FOC with space vector pulse width modulation control algorithm.

The current controller and conversion stages, including PI, Clark transformation, inverse Clark, Park and inverse Parks are shown by the formula below [17].

Clarke Transformation Equation Park Transformation Equation:

$$\begin{bmatrix} i_\alpha \\ i_\beta \end{bmatrix} = \begin{bmatrix} \frac{2}{3} & \frac{-1}{3} & \frac{-1}{3} \\ 0 & \frac{1}{\sqrt{3}} & \frac{-1}{\sqrt{3}} \end{bmatrix} \begin{bmatrix} i_a \\ i_b \\ i_c \end{bmatrix} \quad (8)$$

$$\begin{bmatrix} i_d \\ i_q \end{bmatrix} = \begin{bmatrix} \cos\theta & \sin\theta \\ -\sin\theta & \cos\theta \end{bmatrix} \begin{bmatrix} i_\alpha \\ i_\beta \end{bmatrix} \quad (9)$$

Inverse Park transformation equation

$$\begin{bmatrix} v_\alpha \\ v_\beta \end{bmatrix} = \begin{bmatrix} \cos\theta & -\sin\theta \\ -\sin\theta & \cos\theta \end{bmatrix} \begin{bmatrix} v_d \\ v_q \end{bmatrix} \quad (10)$$

The construction process from the FOC structure is carried out as follows: 1) Measured currents from three stator phases located in the stator reference frame will be converted into two phases using Clarke Transformations; 2) Further converted into the corresponding rotor reference frame using Park Transformation; 3) The obtained outputs from the PI controllers are transformed to inverse Park Transform to obtain the corresponding reference vector for the SVPWM.

C. Space Vector Pulse Width Modulation (SVPWM)

Based on the Patel and Kgiri's research [18], which has given 3 main processes to design for SVPWM:

1) First process: "Sector Identification"

The following algorithm can be used to determine the sector of the reference output voltage vector. Three intermediate variables were considered: V_a, V_b and V_c.

In the first process an algorithm will be given that can be used to determine the area of the reference output voltage vector. Three intermediate variables mentioned are denoted as follows: V_a, V_b, and V_c .

$$V_a = V_\beta; \quad (11)$$

$$V_b = \frac{\sqrt{3}}{2} V_\alpha - \frac{1}{2} V_\beta; \quad (12)$$

$$V_c = \frac{-\sqrt{3}}{2} V_\alpha - \frac{1}{2} V_\beta \quad (13)$$

A, B and C (logical variables) = 0 or 1, depending on the conditions

$$\text{If } Va > 0, A = 1 \text{ else } A = 0; \quad (14)$$

$$\text{If } Vb > 0, B = 1 \text{ else } B = 0; \quad (15)$$

$$\text{If } Vc > 0, C = 1 \text{ else } C = 0 \quad (16)$$

Using the logical variables A, B and C, the variable N is identified as:

$$N = A + 2B + 4C \quad (17)$$

2) Second process: "Calculation of Action Time T_1 and T_2 of Basic Voltage Vector"

In this method, these values were calculated using V_α and V_β. By applying the volt-second balance principle to the orthogonal decay rates of the fundamental vectors, T_1 and T_2 can be mapped from Table I.

where: X, Y and Z are given by:

$$X = \frac{\sqrt{3} V_\beta T_s}{V_{dc}}; \quad (18)$$

$$Y = \left(\frac{3}{2} V_\alpha + \frac{\sqrt{3}}{2} V_\beta \right) \frac{T_s}{2V_{dc}}; \quad (19)$$

$$Z = \left(-\frac{3}{2} V_\alpha + \frac{\sqrt{3}}{2} V_\beta \right) \frac{T_s}{2V_{dc}} \quad (20)$$

TABLE I. THE MAPPING OF X, Y, Z T_0, T_1 AND T_2 [19]

N	C1	C2
1	Z	Y
2	Y	−X
3	−Z	X
4	−X	X
5	X	−Y
6	−Y	−Z

3) Third process: "Determination of $T_{(cm1)}$, $T_{(cm2)}$ and $T_{(cm3)}$"

$T_{(cm1)}$, $T_{(cm2)}$ and $T_{(cm3)}$are the operation times of the three phases. The intermediate variables T_a, T_b and T_c are used to map the comparison values from Table II.

where:

$$T_a = \frac{T - T_1 - T_2}{4}; \quad (21)$$

$$T_b = T_a + \frac{T_1}{2}; \quad (22)$$

$$T_c = T_b + \frac{T_2}{2} \quad (23)$$

TABLE II. THE MAPPING OF T_{CM1} ,T_{CM2} AND T_{CM3} TO T_A , T_B AND T_C [18]

Sector	T_{cm1}	T_{cm2}	T_{cm3}
1	T_b	T_a	T_c
2	T_a	T_c	T_b
3	T_a	T_b	T_c
4	T_c	T_b	T_a
5	T_c	T_a	T_b
6	T_b	T_c	T_a

III. REGENERATIVE BRAKING SYSTEM (RBS)

During urban driving, especially in large cities, vehicles do not move continuously and often stop and start. This is the basis for special attention when determining the effectiveness of regenerative braking.

TABLE III. PARAMETERS USED IN SIMULATION [20, 21]

Block	Parameter	Value	Unit
PMSM	D-axis inductance = Q-axis inductance ($L_d = L_q$)	0.0085	H
	Stator resistance (R_{p-p})	2.875	Ohm
	Poles (p)	4	-
	Flux linkage (ϕ_m)	0.175	Wb
	vehicle mass (m)	2540	kg
VF8 2023 Standard Edition (ECO)	D×R×C	4750×1900×1660	mm
	Wheel radius (r_b)	0.25	m
Battery (lithium-ion) (Prismatic)	Nominal voltage ($V_{nominal}$)	402.8	V
	Cut-off voltage ($V_{cut-off}$)	302.1	V
	Fully Charged voltage	468.854	V

A. Battery (Lithium-ion)

The battery SOC is represented as a percentage (between 0 and 100%). The SOC is calculated as [22].

$$SOC = 100(1 - \frac{1}{Q}\int_0^t i(t)dt) \quad (24)$$

The discharge characteristics of the prismatic Li-ion battery are shown in Fig. 3.

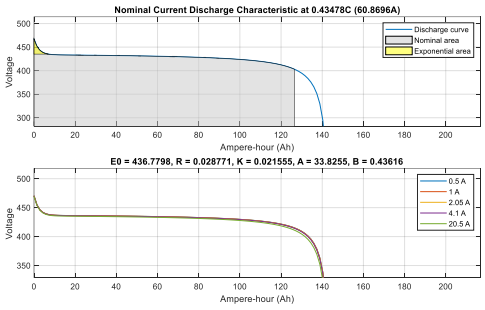

Fig. 3. Discharge characteristics of considered Li-ion battery.

The discharge current for the second graph does not significantly change the values specified for the discharge current parameter [0.5 1 2.05 4.1 20.5] (A) parameter.

B. Drice Cycle Source FTP75

The FTP-75 cycle is a suitable choice for the study of regenerative braking systems due to its realistic representation of urban driving conditions, variability in speed and acceleration and ability to evaluate system performance. The cycle's characteristics make it an ideal platform for testing and evaluating regenerative braking systems and its standardization ensures repeatability and comparability of results. When simulating to obtain optimal results, the author set the simulation time for the cycle to 40 s (Fig. 4.) [23].When simulating to obtain optimal results, the author set the simulation time for the cycle to 40 s [20].

From 0 s to 20 s, the vehicle has a speed of 0 m/s. From 20 s to 33 s, the vehicle accelerates to a maximum speed of 10 m/s. From 33 s to 40 s, the vehicle decelerates to 6.7 m/s.

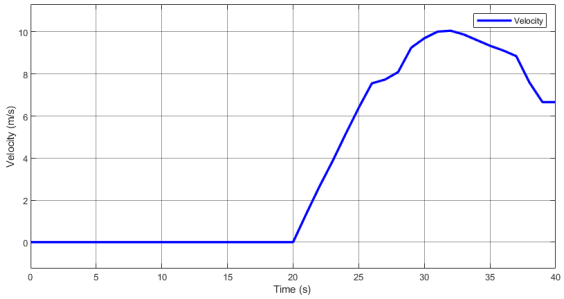

Fig. 4. FTP-75 cycle in 40 s.

C. Determine the Vehicle's Moment of Inertia during Braking or Deceleration

At this time, the torque applied to the active wheel will be Refs. [24, 25]:

Input torque = inertia resistance torque + gradient resistance torque – rolling resistance torque – air resistance torque

$$T_m = i_{rbs} \times \frac{1}{12} \times r_b \times (m\frac{d_v}{d_t}\delta_i - fmgcos\theta_1 - 0.5\rho AC_D(V_t + V_{wind})^2 + mgsin\theta_1) \quad (25)$$

where T_m: Input torque; i_{rbs}: Gear ratio of the energy recovery unit = 0.3; r_b: Tire radius = 0.25 m; m: Car mass kg; δ_i: Coefficient that takes into account the influence of rotating masses referred to the driving wheels = 1; V_t: Car relative velocity; f is the coefficient of rolling resistance = 0.02; g is the acceleration due to gravity = 9.81 m/s^2; θ_1: Gradient angle = 0 rad; ρ: Air density =1.25 kg/m^3; C_D: Coefficient of aerodynamic resistance (drag coefficient) = 0.3; V_{wind}: Wind velocity = 2 m/s; A: Car front area = 2.52 m^2.

After filling in the research data, Fig. 5 is the simulation result given by the author based on the input torque calculation Eq. (25).

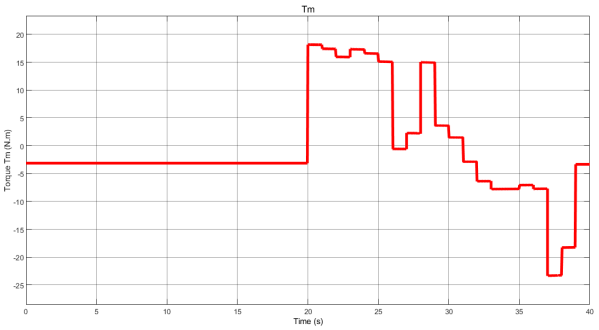

Fig. 5. Input torque, result of mathematical model.

D. PI Control

Researching two articles [26–28] has helped readers better understand the purpose of using and how to implement the three PI controllers to control three interacting variables independently in the model. The system utilizes a cascade control structure with three independent PI modules. The first PI module controls the rotor speed, the second controls the I_q current, and the third controls the I_d current.

where: K_p and K_i is the proportional gain and integral gain of the controller, respectively. The designer needs to choose a set of values $\{K_p\ K_i\}$ that satisfies the control quality to design the PI controller. The calculation method for the PI set is given in Fig. 6.

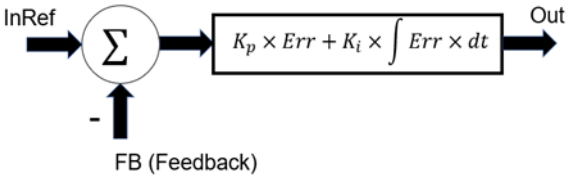

Fig. 6. Principle of operation in the PI adjustment block.

The design of the PI controller is crucial in the digital control of electrical machines, as it significantly impacts control performance. The choice of PI controllers for the given system is justified by their stability, robustness, ability to eliminate steady-state errors, ease of tuning, and reduced oscillations. While PD or PID controllers could be used, the specific requirements of the system and the advantages of PI controllers make them a more suitable choice. This article explores the method of constructing a digital PI controller using the Ziegler-Nichols method to find the controller's proportional gain K_p and integral time constant K_i. The obtained K_p and K_i coefficients are then used in the PI control block to regulate the speed of the PMSM [29].

E. Simulation Model

The model, which includes: lithium-ion battery, three-phase IGBT inverter, PMSM, control subsystem and related blocks, considers factors affecting the braking torque of the vehicle, such as the vehicle's moment of inertia, gradient resistance torque, rolling resistance torque and air resistance torque [30–33].

The study simulates driving a vehicle through a real FTP-75 cycle at speeds and accelerations consistent with international standards. The input block uses the velocity and acceleration values from the cycle to calculate rolling resistance, gradient resistance, air resistance, and inertia forces. These forces are then converted into torque acting on the wheel by multiplying by the wheel's radius. Next, the torque is transmitted through the gearbox and differential to the PMSM.

The motor control system uses a two-loop structure with speed and current feedback. The speed control loop plays a crucial role, allowing the motor to reach its desired speed, maintain close adherence to the specified input signal and achieve speed control without static error. Additionally, the closed-loop nature of the speed control loop provides good resistance to sudden load changes. The current control loop primarily serves as a protection circuit to limit current and prevent overload, while also suppressing network voltage disturbances. When starting and braking, the motor can operate at its maximum current rating, allowing the system to quickly reach a steady state. According to the two-loop control structure and the control mode $i_d = 0$, the system model is set up as shown in Fig. 7. The system consists of PI speed and current controllers, Park and Clarke transforms, a pulse width modulator (PWM), a motor model, current sensors, and speed sensors. Both PI controllers have limited output signals. Matlab/Simulink is used for simulation; the simulation time is 40 s. The system starts without load, and the initial rotor speed is 1000 rpm.

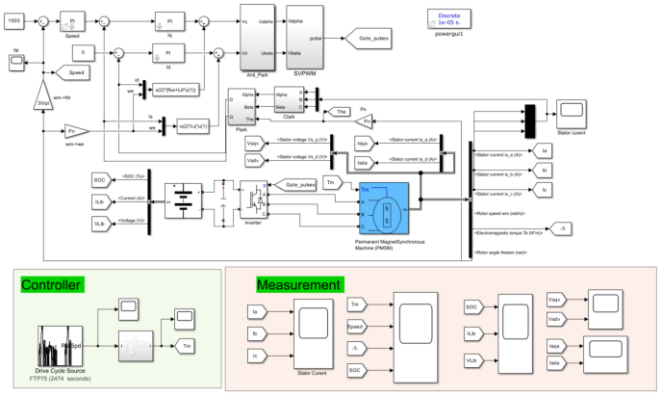

Fig. 7. Simulation model of regenerative braking system.

On the VINFAST VF8 electric vehicle, the Regenerative Braking System (RBS) utilizes motors/generators operating in various constant or alternating voltage modes. The recovered energy during braking is stored in the prismatic battery. This RBS system with a prismatic battery is commonly used in electric and hybrid vehicles and requires power converters.

The inverter is modeled using an RLC circuit and a current inverter that receives control signals to the gates ($Gate_{pulses}$) to modulate the output voltage on phases A, B and C, feeding the motor.

Simulation results demonstrate the performance of the regenerative braking system and the parameters associated

with the lithium-ion battery and permanent magnet synchronous motor when using the FTP-75 cycle for 40 s.

IV. Simulation Results

The electromagnetic torque of the simulated PMSM is shown in Fig. 8. From this figure, it can be seen that the electromagnetic torque generally follows the shape of the input torque but experiences short periods of oscillation due to the exported inertia whenever the value of the input torque changes.

The model was simulated for 40 s, and the simulation parameters were taken according to the specifications of the VF8 2023 Standard Edition (ECO) electric vehicle. The input mechanical torque has an amplitude calculated based on Eq. (25). The amplitude varied between 20 N·m for propulsion and −23 N·m for braking.

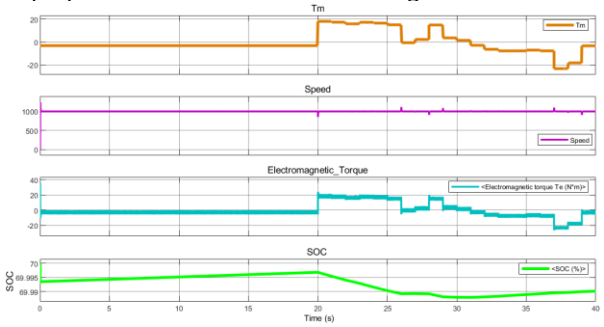

Fig. 8. Input torque reference, rotor speed, electromagnetic torque, battery's SOC.

The positive values (+) of the input torque operate the PMSM as a motor in the time range of 20 s to 33 s (as evidenced by the State of Charge (SOC) value decreasing from 69.997% to 69.987%). The negative values (-) of the input torque operate the PMSM as a generator during two time periods: from 0 s to 20s and from 33 s to 40 s (with the SOC value increasing from 69.994% to 69.997% and from 69.987% to 69.99%, respectively).

The battery capacity percentages are shown in Fig. 9. This figure includes three graphs. The first graph shows the relationship between the battery's State of Charge (SOC) and time. The second and third graphs show the time relationship of the battery's current $i_{(t)}$ and voltage $V_{batt(t)}$.

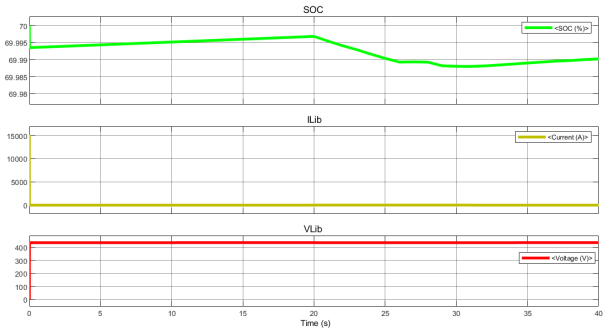

Fig. 9. Battery's SOC, current, and voltage.

- SOC Trend (Top Graph): The SOC graph indicates a general downward trend, signifying battery discharge during the observed period. The relatively gradual decrease suggests a moderate power demand. The noticeable dip around the 20-second mark signifies a period of increased power draw. This could correspond to events like acceleration, going uphill or activating a high-power accessory. Monitoring the long-term SOC trend is crucial for estimating remaining range and planning operations effectively.
- Current Profile (Middle Graph): The current graph shows a relatively stable, low current draw for most of the observation period. The prominent spike around the 20-second mark confirms the increased power demand observed in the SOC graph. The magnitude of this current spike is a key indicator of the power being delivered by the battery at that moment. Understanding the typical current profile under various operating conditions is essential for designing effective thermal management systems and optimizing battery usage patterns.
- Voltage Response (Bottom Graph): The battery voltage remains relatively stable throughout the observation period with a slight dip coinciding with the current spike around the 20-second mark. This voltage drop is expected under increased load due to the battery's internal resistance.

Fig. 10 shows a graph with two subplots, each representing a different axis current (d-axis and q-axis) over time. The top subplot displays the d-axis current, which fluctuates around a central value close to zero, indicating that the d-axis current is primarily responsible for maintaining the magnetic field in the motor. The bottom subplot shows the q-axis current, which exhibits larger fluctuations, reflecting the torque production in the motor. The q-axis current's behavior aligns with the electromagnetic torque equation, where changes in this current directly influence the torque output. All results given are consistent with the author's choice when selecting the SPMSM engine.

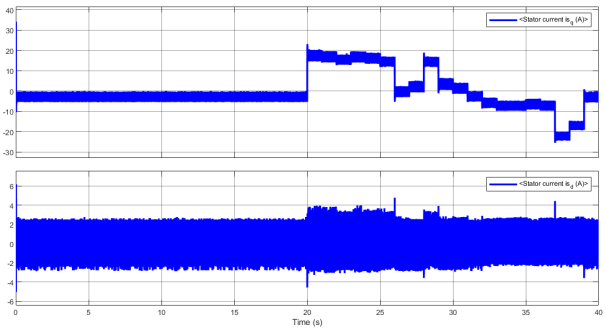

Fig. 10. Stator curent i_q, Stator curent i_d.

V. Conclusion

This article has presented a detailed simulation model of a regenerative braking system designed for the VinFast VF8 2023 Standard Edition (ECO) electric vehicle. The model incorporates a prismatic lithium-ion battery, a current converter, and a permanent magnet synchronous motor (PMSM). The implementation of Field-Oriented

Control (FOC), in conjunction with a Proportional-Integral (PI) controller, effectively minimizes torque and current ripples, enhancing overall system efficiency. Space Vector Pulse Width Modulation (SVPWM) is employed to precisely control motor speed and ensure optimal energy recovery during braking.

Simulation results, based on a 40-second segment of the FTP-75 drive cycle, demonstrate the effectiveness of the proposed system. During braking periods, when the input torque is negative, the PMSM successfully transitions to generator mode, increasing the battery's State of Charge (SOC) by approximately 0.003%. The power converter effectively functions as a rectifier, channeling the recovered energy back into the battery. The FOC control, combined with the PI current controller, ensures precise regulation of the PMSM's output torque, closely adhering to the input reference. As anticipated for a Surface-mounted Permanent Magnet Synchronous Machine (SPMSM) with equal d- and q-axis inductances ($Ld = Lq$), the d-axis current (i_d) remains near zero. Furthermore, the SVPWM control strategy effectively manages the system's dynamic response, preventing overspeeding and demonstrating its robustness for real-world application.

These findings, while based on a short simulation period, demonstrate the significant potential of regenerative braking to recapture energy normally lost during deceleration in EVs. The observed increase in battery SOC, even over a brief driving segment, highlights the feasibility and effectiveness of using SVPWM control in the VinFast VF8 2023 Standard Edition (ECO) to enhance its energy efficiency. By extending driving range and reducing reliance on external charging, this technology plays a crucial role in addressing range anxiety and promoting the wider adoption of electric vehicles. This research therefore contributes valuable insights to the ongoing development of more efficient and sustainable transportation solutions.

Conflict of Interest

The authors declared no potential conflicts of interest with respect to the research, authorship and publication of this article.

Author Contributions

Vu Hai Quan proposed the conceptual idea and theoretical model. Nguyen Trong Duc conducted the simulation and drafted the manuscript. Hoang Quang Tuan and Vu Hai Quan reviewed the manuscript and finalized the article. All authors discussed the results, reviewed, and approved the final version of the manuscript. The completed manuscript was the result of contributions from all authors. All authors had approved the final version.

References

[1] Z. Wang, L. Hu, F. Wang, M. Lin, and N. Wu, "Assessing the impact of different population density scenarios on two-wheeler accident characteristics at intersections," *Sustainability*, vol. 16, 1737, 2024. https:// doi.org/10.3390/su16051737

[2] Data World Health Organization. (2023). [Online]. Available: https://www.who.int/teams/social-determinants-of-health/safety-and-mobility/global-status-report-on-road-safety-2023

[3] V. H. U. Eze, E. Edozie, K. Umaru, O. O. Wisdom, U. Chinyere N, and O. F.Chukwudi, "Overview of renewable energy power generation and conversion (2015–2023)," *Eurasian Experiment Journal of Engineering (EEJE)*, vol. 4, issue 1, 2023.

[4] N. Kh. Tuan, K. E. Karpukhin, A. S. Terenchenko, and A. F. Kolbasov, "World trends in the development of vehicles with alternative energy sources," *ARPN Journal of Engineering and Applied Sciences*, vol. 13, no. 7, pp. 2535–2542, 2018.

[5] R. P. Narasipuram and S. Mopidevi, "Assessment of e-mode GaN technology, practical power loss, and efficiency modelling of iL2C resonant DC-DC converter for xEV charging applications," *Journal of Energy Storage*, vol. 91, June 30, 2024. https://doi.org/10.1016/j.est.2024.112008

[6] R. P. Narasipuram and S. Mopidevi, "An industrial design of 400 V–48 V, 98.2% peak efficient charger using E-mode GaN technology with wide operating ranges for xEV applications," *International Journal of Numerical Modelling: Electronic Networks, Devices and Fields*, vol. 37, issue 6, 2023. https://doi.org/10.1002/jnm.3194

[7] A. Terenchenko, K. Karpukhin, and R. Kurmaev, "Features of operation of electromobile transport in the conditions of Russia," in *Proc. 28th International Electric Vehicle Symposium and Exhibition (EVS 2015)*, 2015.

[8] A. E. Korial and I. I. Gorial, "System analysis and controllers performance comparison for D.C. motor," *International Journal of Mechanical Engineering and Robotics Research*, vol. 11, no. 7, pp. 520–526, Jul. 2022. doi: 10.18178/ijmerr.11.7.520-526

[9] B. Plangklang, S. Kantawong, and A. Noppakant, "Study of generator mode on Permanent Magnet Synchronous Motor (PMSM) for application on Elevator Energy Regenerative Unit (EERU)," *Energy Procedia*, vol. 34, pp. 382–389, 2013. doi: 10.1016/j.egypro.2013.06.766

[10] C. He and T. Wu, "Analysis and design of surface permanent magnet synchronous motor and generator," *CES Transactions on Electrical Machines and Systems*, pp. 94–100, 2019. doi: 10.30941/CESTEMS.2019.00013

[11] A. Abdenour, "Optimal design of an interior permanent magnet synchronous motor for wide constant-power region operation: Considering thermal and electromagnetic aspects," *SAE International Journal of Alternative Powertrains*, pp. 129–138, 2014. doi: 10.4271/2014-01-1889

[12] N. Gujjula and G. Laxminarayana, "Field-oriented control of PMSM drive based on SVPWM using MATLAB," *International Journal of Engineering Research and Applications*, vol. 4, no. 7, pp. 95–99, Jul. 2014

[13] V. Totev and V. Gueorgiev, "Modelling of regenerative braking," in *Proc. 2021 17th International Conference on Electrical Machines, Drives and Power Systems (ELMA)*, Sofia, Bulgaria, Jul. 2021.

[14] A. M. Tom and J. L. F. Daya, "Machine learning techniques for vector control of permanent magnet synchronous motor drives," *Cogent Engineering*, vol. 11, no. 1, 2323813, 2024. doi: 10.1080/23311916.2024.2323813

[15] X. Liu, J. Du, and D. Liang, "Analysis and speed ripple mitigation of a space vector pulse width modulation-based permanent magnet synchronous motor with a particle swarm optimization algorithm," *Energies*, vol. 9, no. 11, 923, 2016. doi: 10.3390/en9110923

[16] K. Sumitra, M. Suresh, and M. K. Giridharan, "PMSM field oriented control using SVPWM for control moment gyroscope (CMG)," *International Journal of Engineering Research & Technology*, vol. 4, no. 8, Aug. 2015.

[17] K. Sumitra and M. K. Giridharan, "Comparison between field oriented control of BLDCM and PMSM using SVPWM in minimizing torque ripples in satellite application," *International Journal for Scientific Research & Development*, vol. 3, no. 9, 2015.

[18] V. Patel and V. Kgiri, "Field oriented control of PMSM drive using SVPWM technique," *International Journal of Engineering Research and Applications*, vol. 2, no. 3, pp. 246–255, Jun. 2014.

[19] P. Kumar, M. Kumar, and S. Dahiya, "Sensorless speed control of PMSM using SVPWM technique based on MRAS method for various speed and load variations," in *Proc. the World Congress on Engineering (WCE)*, London, UK, Jul. 2015.

[20] Data Vinfast. (2023). [Online]. Available: https://www.autofun.vn/tin-tuc/change-battery-format-vinfast-vf-8-now-100-kg-lighter-improves-performance-68001

[21] T.-T. Liu, Y. Tan, G. Wu, and S.-M. Wang, "Simulation of PMSM vector control system based on Matlab/Simulink," in *Proc. 2009 International Conference on Measuring Technology and Mechatronics Automation*, 2009. doi: 10.1109/ICMTMA.2009.117

[22] Data MatWorks. (2024). [Online]. Available: https://es.mathworks.com/help/physmod/sps/powersys/ref/battery.html

[23] S. Kang and K. Min, "Dynamic simulation of a fuel cell hybrid vehicle during the federal test procedure-75 driving cycle," *Applied Energy*, vol. 161, pp. 181–196, 2016. doi: 10.1016/j.apenergy.2015.09.093

[24] A. S. Terenchenko, K. E. Karpukhin, A. A. Shorin, and S. F. Sklyarinskiy, "Optimizing the losses in a tractional induction motor within a hybrid system," *Russian Engineering Research*, vol. 35, no. 3, pp. 171–173, 2015. doi: 10.3103/S1068798X15030193

[25] A. Kolbasov *et al.*, "Analytical study of the power parameters of electric traction drive for modern vehicles," *Lecture Notes in Networks and Systems*, vol. 178, pp. 200–209, 2021.

[26] B. Fecko and A. Kalinov, "MATLAB model and PI controller of DC permanent magnet motor," in *Proc. 2019 IEEE International Conference on Modern Electrical and Energy Systems (MEES)*, Kremenchuk, Ukraine, Sep. 2019, pp. 370–373. doi: 10.1109/MEES.2019.8896578

[27] T. Doğruer and N. Tan, "Design of PI controller using optimization method in fractional order control systems," *IFAC-PapersOnLine*, vol. 51, no. 4, pp. 841–846, 2018. doi: 10.1016/j.ifacol.2018.06.124

[28] T.-Y. Jeon and B.-G. Jung, "A study of PI controller tuning methods using the internal model control guide for a ship central cooling system," *Journal of Marine Science and Engineering*, vol. 11, no. 10, 2025, 2023. doi: 10.3390/jmse11102025

[29] V. H. Quan *et al.*, "Modelling and simulation of automatic brake system of vehicle," *ARPN Journal of Engineering and Applied Sciences*, May 2023. doi: 10.59018/0423116

[30] W. L. and P. X., "Design of PMSM speed control system based on Simulink model," *IOP Conference Series: Materials Science and Engineering*, vol. 569, 042004, 2019. doi: 10.1088/1757-899X/569/4/042004

[31] N. V. Quỳnh, H. T. Nga, N. H. Huy, and L. H. Sơn, "Co-simulation and experiment PMSM speed controller with vector control and SVPWM algorithm based on FPGA," *Journal of Science of Lac Hong University*, vol. 4, pp. 53–58, Dec. 2015.

[32] V. H. Quan *et al.*, "Design an intelligent braking system using ultrasonic sensors and IR sensors," in *Proc. the 3rd Annual International Conference on Material, Machines and Methods for Sustainable Development (MMMS2022)*, Springer, 2024. doi: 10.1007/978-3-031-57460-3_36

[33] V. H. Quan, L. T. Long, N. A. Ngoc, and N. M. Tien, "A comparison of the performance of anti-lock braking system (ABS) using fuzzy and PID controllers," in *Proc. 2022 6th International Conference on Green Technology and Sustainable Development (GTSD)*, Nha Trang, Vietnam, 2022, pp. 243–248. doi: 10.1109/GTSD54989.2022.9989135